


Scaffold Adhering to Peptide-Based Biomimetic Extracellular Matrix Composite Nanobioglass Promotes the Proliferation and Migration of Skin Fibroblasts Through the GSK-3 β / β -Catenin Signaling Axis

Kun Cao^{1,2,*}, Zehui Wang^{1,3,5,6,*} , Xiaojiao Sun^{3-6,*}, Di Yan¹⁻³, Yanwen Liu³, Ting Ma³, Xiaojuan Sun^{1,2}

¹Department of Oral and Maxillofacial Surgery, General Hospital of Ningxia Medical University, Yinchuan, Ningxia, 750004, People's Republic of China; ²Institute of Medical Sciences, General Hospital of Ningxia Medical University, Yinchuan, Ningxia, 750004, People's Republic of China; ³School of Stomatology, Ningxia Medical University, Yinchuan, Ningxia, 750004, People's Republic of China; ⁴Animal Experiment Center of Ningxia Medical University, Ningxia Medical University, Yinchuan, Ningxia, 750004, People's Republic of China; ⁵Stem Cell Institute, General Hospital, Ningxia Medical University, Yinchuan, Ningxia, 750004, People's Republic of China; ⁶Ningxia Key Laboratory of Clinical and Pathogenic Microbiology, General Hospital of Ningxia Medical University, Yinchuan, Ningxia, 750004, People's Republic of China

*These authors contributed equally to this work

Correspondence: Zehui Wang, Department of Oral and Maxillofacial Surgery, General Hospital of Ningxia Medical University, Yinchuan, Ningxia, 750004, People's Republic of China, Email wangzehui364@163.com; Xiaojuan Sun, Department of Oral and Maxillofacial Surgery, General Hospital of Ningxia Medical University, Yinchuan, Ningxia, 750004, People's Republic of China, Email ms_sunxiaojuan@126.com

Introduction: Nano-mesoporous bioactive glass and RGD peptide-coated collagen membranes have great potential in wound healing. However, the application of their compound has not been further studied. Our purpose is to prepare a novel bioactive collagen scaffold containing both NMBG stent and adhesion peptides (BM), which then proves its promising prospect the assessment of physical properties, biocompatibility, GSK-3 β / β -catenin signaling axis and toxicological effects.

Methods: The structural and morphological changes of BM were analyzed using scanning electron microscopy (SEM) and Energy Dispersive Spectroscopy (EDS). In vivo, wound healing of BM was assessed in SD rats through dynamic monitoring and calculation of wound healing rate. Immunohistofluorescence (IHF), H&E, and Masson staining were utilized; in vitro, primary cell culture, and a variety of assays including CCK-8, Transwell, Scratch, Immunocytofluorescence (ICF), and Western blot (WB) were performed, both for morphology and molecular analysis.

Results and Discussion: Preparation of BM involved attaching NMBG to RGD-exposed collagen while avoiding the use of toxic chemical reagents. BM exhibited a distinctive superficial morphology with increased Si content, indicating successful NMBG attachment. In vivo studies on SD rats demonstrated the superior wound healing capability of BM, as evidenced by accelerated wound closure, thicker epithelial layers, and enhanced collagen deposition compared to the NC group. Additionally, BM promoted skin fibroblast migration and proliferation, possibly through activation of the GSK-3 β / β -catenin signaling axis, which was crucial for tissue regeneration. This study underscored the potential of BM as an effective wound-healing dressing.

Conclusion: A new method for synthesizing ECM-like membranes has been developed using nano-mesoporous bioactive glass and collagen-derived peptides. This approach enhances the bioactivity of biomaterials through surface functionalization and growth factor-free therapy.

Keywords: NMBG, proliferation, RGD, migration, wound healing, GSK-3 β / β -catenin signaling axis

Introduction

For healing wounds, the skin has developed four main phases of sophisticated mechanisms: hemostasis, inflammation, proliferation, and remodeling of the extracellular matrix (ECM).^{1,2} Fibroblasts, the main cell type responsible for ECM

remodeling, produces collagen and other biological components.³ Fibroblasts, which are the main component cells of the dermis, participate in the process of wound healing and tissue remodeling after skin injury.⁴ The migration of fibroblasts and the extracellular matrix they secrete are vital for wound healing and tissue repair.⁵ Furthermore, Collagen, the most abundant protein in the extracellular matrix of human skin, has shown the ability to enhance cell migration and proliferation, making it integral to wound healing and promoting fibroblasts' proliferation. It plays an important role in interacting with cells and regulating the wound healing process.⁶ The lack of collagen also poses a significant challenge in terms of its modification and organization, which can impair wound healing.⁷ Mistry et al assessed in vitro wound closure of Col 1 peptides. The results showed that collagen peptides significantly promoted wound closure in fibroblasts' proliferation and ki67 expression.⁸

RGD, found in the extracellular matrix (ECM), is a multifunctional cell attachment site in fibronectin and other proteins.⁹ It has been used in grafting onto synthetic and natural materials to enhance cell proliferation and organization for regeneration.^{10,11}

RGD facilitates the interaction between cells and their microenvironment by providing binding sites within the ECM. This interaction plays an essential role in regulating various cellular processes such as proliferation, migration, growth factor sequestration, and cell signaling through cell surface receptors.¹²

Yakovlev et al conducted experiments demonstrating that RGD promotes wound closure in HUVEC by interacting with the α C domain of the HUVEC integrin binding site.¹³ In our study, we utilized nanobioactive glass as a cell scaffold to investigate the migration and healing of fibroblasts. This approach addressed the limitations of insufficient thickness and rapid degradation observed in commercial collagen membranes. Moreover, it accelerated the speed of fibroblasts spreading and migration. Additionally, we were able to control the release rate of RGD to maintain its natural activity.¹⁴

In their study on the thermal stability of collagen, Kronick et al utilized subcutaneous reticular collagen tissue extracted from cattle. They subjected the tissue to heat at 68°C for 75 minutes and observed that half of the collagen underwent deconstruction, resulting in the formation of the adhesive polypeptide RGD.¹⁵

Compared to pure collagen, the mixed structure of polypeptide and collagen serves the dual purpose of maintaining scaffold stability and enhancing biological activity. The RGD sites of integrin binding in the injured area become exposed to adhesion peptide molecules, thus contributing to the wound healing process.^{16,17} Consequently, the mixed membrane comprising the peptide adhesion sequence RGD/collagen can be viewed as a simplified extracellular matrix (ECM) model.¹⁸

In general, we propose a method to expose the polypeptide adhesion sequence RGD in its natural form to the biological collagen film by appropriately heating it, while ensuring the stability of the collagen membrane, retaining at least 50% of its original structure. The RGD sequence derived from collagen denaturation is not modified or contaminated with any additional substances or chemical cross-linking agents. By conjugating the RGD to the surface of the material, the collagen membrane becomes stronger and safer. Fixed RGD sequence on the material's surface promotes cell attachment, while free RGD dissolved in the solution inhibits cell anchoring.¹⁹ Moreover, we embed the RGD sequence in nano-mesoporous bioactive glass (NMBG) within the collagen membrane scaffold. Organic material compounding frequently involves the use of NMBG scaffolds to enhance the properties of raw materials.

NMBG is always used as a scaffold, in regenerative medicine, and drug delivery in tissue engineering.^{20–22} In a previous work, NMBG was fabricated by dry ChG sponge scaffolds modified with nano bioactive glass and nano-mesoporous bioactive glass possessed excellent cytocompatibility, bone-like apatite induction in vitro, and bone regeneration capacity in vivo.²³ These scaffolds have the capability to promote cell adhesion, proliferation, and differentiation in vitro. When mesoporous bioactive glass comes into contact with body fluids, the high specific surface area and mesoporous structure of bioactive glass react rapidly. This reaction leads to the formation of a scaffold with hydroxyapatite product.²⁴ NMBG also allows for a gradual release of the cell adhesion-promoting polypeptide sequence during the degradation of the collagen membrane scaffold.²⁵

However, the effect of RGD-loaded NMBGylated collagen membrane scaffolds on the proliferation and migration of fibroblasts in skin connective tissue has not been investigated yet. Our previous research has demonstrated that the Wnt signaling pathway plays a crucial role in the proliferation and migration of fibroblasts, influencing the repair and regeneration of soft tissue through the regulation of key processes such as cell proliferation, migration, and Extra

Cellular Matrix (ECM) synthesis. Additionally, our research group has previously shown that biomimetic extracellular matrix collagen membranes containing BFGF and RGD can enhance the adhesion and proliferation of skin fibroblasts.²⁶

Some researchers have suggested that different concentrations of RGD can regulate cell movement and have analyzed the relationship between osteoblast differentiation and cell migration, as well as the involvement of the Wnt signaling pathway.²⁷ Activation of the Wnt signaling pathway leads to the phosphorylation of GSK-3 β protein, allowing β -catenin to enter the nucleus and promote growth signals for controlling cell behavior.²⁸

In the end, our study prepared a bioactive BM containing NMBG stent and adhesion peptides. We are supposed to prove the novelty and promising prospect of wound healing biomaterials, through the assessment of physical properties, biocompatibility, and toxicological effects after incorporating RGD and NMBG.

Methods

BM Production

Dissolve 4 g of PEO-PPO-PEO in 20 mL of ethanol and sonicate the mixture for 5 minutes until it is completely dissolved. Then, add 6.7 g of TEOS, 0.73 g of TEP, and 0.6580 g of CaCl₂ into the solution and stir with a Vortex Mixer (Servicebio, China) for 30 minutes vigorously. Subsequently, add 55mL HCl (0.5 mol/L) into the former liquid and place the final mixture overnight.

A commercial collagen membrane, CO (Heal-all membrane, ZH-BIO, China), was exposed to denaturation at 122°F and 30% humidity for 1 hour.

Two milliliters of the final mixture was evenly applied on the RGD exposed membrane in a culture dish via a dropper. The membrane would be dried in an oven at 86°F for 2 hours. After repeating this process three times, the membrane was dried at room temperature for 24 hours.

To prepare the NMBG-embedded RGD biomimetic extracellular matrix (BM), the last step was to soak the membrane in a mixed solution (1 mL of 37% HCl and 99 mL of ethanol) at a constant temperature water bath at 98.6°F for 24 hours, and totally dried BM at room temperature.

Scanning Electron Microscope (SEM)

CO, RGD exposed CO, and BM were cut to a size of 0.5 mm * 0.5 mm. Then, we sprayed gold on the prepared membrane for electron microscope specimens and observed the materials under a scanning electron microscope. The morphology of the surfaces was recorded by field-emission scanning electron microscopy (FESEM, FEI Quanta FEG 250, 20 kV, USA).

Energy-Dispersive Spectrometer (EDS) of BM

CO and BM samples were prepared into 0.5 mm * 0.5 mm. We used Energy-Dispersive Spectroscopy (EDS) to identify the qualitative and quantitative analysis of C, N, O, Si, P, Cl, and Ca elements (EDAX, INC, Genesis APEX APOLLO X, 20 kV, USA) and analyzed the differences among the elements by GraphPad Prism 9.

In vivo Wound Healing of BM

SD rats were obtained from the Experimental Animal Center of Ningxia Medical University (IACUC-NYLAC-2022-207, Yinchuan, Ningxia, China). The rats were maintained under SPF-level barrier conditions, and all procedures were approved by the Experimental Animal Care and Experimentation Committee of Ningxia Medical University. The study followed ARRIVE guidelines and adhered to the 4R principles. All experimental operations were performed under inhalation anesthesia using 5% isoflurane for induction anesthesia and 1% for maintenance anesthesia. Minimal measures were taken to alleviate discomfort and pain during the operation. When the animals woke up, they were kept warm, and their vital signs were monitored before being returned to their cages, minimizing the influence of non-experimental factors. After anesthesia and fur removal, a total of 27 SD rats (3w) were randomly divided into three groups. The backs were disinfected with 75% alcohol, and a full-thickness skin resection (d=1cm) was removed from the back. The NC (Negative Control) group served as the negative control group treated with physiological saline, while the CO and BM

groups were treated as positive control and experimental groups, respectively. Photos were taken with a digital camera to record the dynamic changes of the wounds on the 3rd, 7th, and 14th day.

Wound healing rate formula: $\text{wound healing rate}(\%) = (1 - A_n/A_0) \times 100\%$

(A_0 : wound surface area at 0 day; A_n : wound surface area at 3rd day, 7th, day, 14th day)

HE & Masson

To evaluate the histological changes, the back wound of the 3rd, 7th, and 14th day and important organs (heart, liver, spleen, kidney, and lung) were cut for H&E and Masson staining. Additionally, the weight of the SD rats and important organs were recorded for H&E staining, in order to detect potential toxicity. The proportion of important organs in the body weight of SD rats was calculated using the formula:

$\text{Proportion of important organs}(\%) = (\text{heart} + \text{liver} + \text{spleen} + \text{kidney} + \text{lung}) / \text{SD rat weight} \times 100\%$

All skin and organ samples were placed in 10% paraformaldehyde fixative, then dehydrated, made transparent, immersed in wax, and embedded in 4um paraffin sections. Skin sections were stained with H&E and Masson to examine changes in the wound-healing process of soft tissue, such as epithelial regeneration, granulation tissue, and collagen deposition. Organ sections were stained with H&E staining to assess the in vivo toxicity of the materials.

Immunohistofluorescence (IHF)

Three groups of paraffin samples (NC, CO, and BM) were taken on the 14th day. Paraffin sections of 4um thickness were made and then baked, dewaxed, and hydrated. Antigen retrieval was performed, followed by incubation with 0.3% PBST (Triton X-100) at room temperature for 15 minutes. The sections were sealed with a goat serum of working solution. Primary antibodies Ki67 (Servicebio, China) and Col 1 (Abcam, UK) were applied, followed by secondary antibodies (Abclonal, China). The sections were observed using an inverted fluorescence microscope (Nikon, Japan), and three fields of view were randomly selected for recording.

Primary Cell Culture of SD Rat Skin Fibroblasts

Full-thickness back skin samples from SD rats were taken after anesthesia. The samples were placed in DMEM (Gibco, US) with 1 mg/mL Dispase II (Solarbio, China), and kept at 39.2°F for 18 hours. Afterward, 1 mg/mL Type I collagenase (Solarbio, China) was added at 98.6°F for 1 hour to remove the epithelial layer. The skin was cut into 1 mm * 1 mm pieces and centrifuged at 1500 rpm/min for 5 minutes. The left cells were inoculated into T25 culture flasks and incubated upside down for 3 hours. Subsequently, the cells were cultured with 15% FBS (Viva Cell BIOSCIENCES, Israel) for 3 passages. After 6 passages, primary skin fibroblasts were purified. The purified cells were observed and photographed using an inverted fluorescence microscope (Nikon, Japan) to record their bright field and fluorescence morphology.

CCK-8

The 6th-generation cells were seeded into a 96-well plate at a density of 5×10^3 cells per well. After the cells adhered, they were starved for 12 hours. Each well was then added with 100ul of complete culture medium in the NC group, BM group containing 1, 5, 10ug/mL, and 10ug/mL BM+100ng/mL DKK-1 group. The cells were cultured for 24h and 48h, respectively, and were then detected using the CCK-8 kit (NCM Biotech, China). The absorbance value at 450 nm was measured using a microplate reader (Bio-Rad, US) and recorded.

Transwell

TrypLE™ Express (Thermo Fisher SCIENTIFIC, US) was used to digest skin fibroblasts which were then resuspended with DMEM. The cell density was adjusted to 3×10^4 / mL, and 100μL of the mixed cell suspension was added to the upper chamber coated with gel. In the lower chamber, the NC group was cultured with 700ul DMEM (10% FBS). The CO group was in 700 ul of DMEM (10% FBS+10ug/mL CO), while the BM group was cultured with 700 ul (10% FBS +10ug/mL BM) for 12 hours. After removing the upper chamber, it was rinsed with 4% Paraformaldehyde Fix Solution

for 30 min then kept in 0.5% crystal violet aqueous solution at room temperature for 15 minutes. Wash and dry the chamber. Three fields of view were randomly selected in each well to capture images. Cell counting was performed using Image J software, and statistical analysis was conducted using GraphPad Prism 9.0.

Scratch

The skin fibroblasts were seeded in a 6-well plate at a density of 1×10^5 . Once the fusion reached 80%, the 10ul pipette tip perpendicular to the bottom of the well was used to make a scratch. Subsequently, the cells were washed with PBS and divided into three groups: NC group, CO group, and BM group. Pictures were taken at the 0, 12th, and 24th hours using an inverted microscope (Nikon, Japan) to record the closure of the scratches. The area of scratch healing was calculated using Image J software, and statistical analysis was performed using GraphPad Prism 9.0.

Immunocytofluorescence (ICF)

The 6th-generation cells were seeded on a 24mm cell slide at a concentration of 1×10^5 . After adhesion, the cells were starved for 12 hours. Added the complete culture medium (NC group), complete culture medium along with 10ug/mL CO (CO group), and complete culture medium 10ug/mL BM (BM group) to culture cells. After 48 hours, the cells were fixed with 4% paraformaldehyde, permeabilized, and followed by primary antibodies Vimentin (Abcam, U.K.), Ki67 (Servicebio, China), and Col 1 (Abcam, U.K.), Secondary antibodies (Abclonal, China). Mount the slide with Dapi anti-fade reagent. Record 3 fields of view randomly via inverted fluorescence microscope (Nikon, Japan).

WB

The cells were seeded in a 100mm culture dish at a concentration of 1×10^7 . They were divided into three groups: NC, BM (10%FBS+10ug/mL BM), and DKK-1 (BM+DKK-1). The DKK-1 group contained a combination of 10%FBS, 10ug/mL BM, and 100ng/mL DKK-1. After three days of culture, the proteins were extracted for SDS-PAGE electrophoresis. Primary antibodies β -catenin (Abcam, U.K.), GSK-3 β (Abcam, UK), p-GSK-3 β (Abcam, UK), and GAPDH (Abclonal, China), before secondary antibodies (Abclonal, China), were applied. AI680 (Cytiva, US) was used for exposure.

Statistics Method

In this study, the data is shown as mean \pm SD and evaluated using GraphPad Prism 9 by One-way ANOVA and two-way ANOVA for at least three times. $P < 0.05$ was considered as statistically significant, and * = $p < 0.05$, ** = $p < 0.01$, *** = $p < 0.001$, **** = $p < 0.0001$ in the histogram indicated that there was no statistical difference with ns or without *.

Figures

Figure 1 was created using the Figdraw website, with the authorization ID: ASWPY9dd23. From Figures 2–7, the figures were managed by Adobe Photoshop 2022.

Result and Discussion

Preparation of BM

Figure 1 shows the BM production process. After exposing RGD, NMBG was attached to the bionic collagen membrane, resulting in the formation of a bionic collagen membrane BM with NMBG wrapping RGD.

In the process of BM, Glutaraldehyde, a common cross-linking agent with absolute toxicity, was not used. Research has shown that proteolysis or heating could cause partial denaturation of type I collagen, leading to the exposure of the linear RGD cell adhesion sequence.²⁹ Preosteoblasts were spread on collagen that had been thermally denatured and heated for 1 hour, as well as on natural collagen that had not been denatured. After 14 minutes, it was observed that 50% of the cells adhered and spread on the denatured collagen, which was twice as fast as on natural collagen. It was suggested that the organizational transformation may occur later.³⁰ Furthermore, heating and denaturing collagen did not affect the fibrous framework or the arrangement of macromolecular collagen.

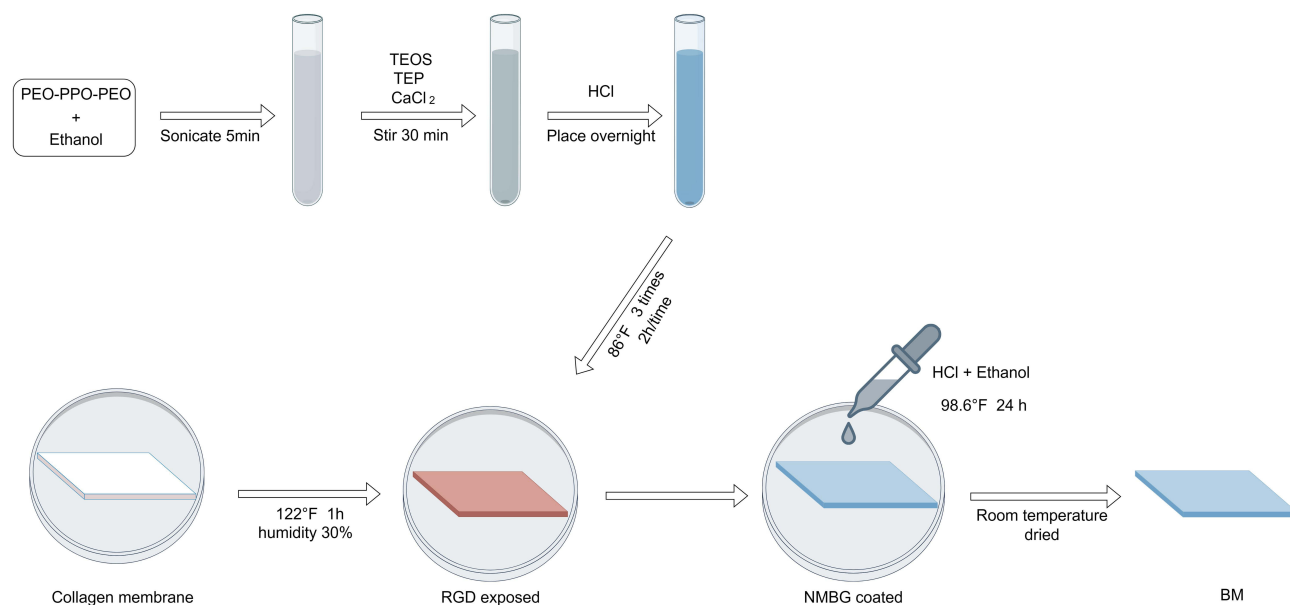


Figure 1 The process of making BM.

Morphological Characterization Comparison Included Surface Feature and Content of Inorganic Element

Figure 2A shows the evaluation of the surface morphology and complex three-dimensional microstructure of the CO Membrane, RGD-exposed Membrane, and NMBG Coated Membrane (BM).

The SEM image (**Figure 2A**) revealed that the smooth collagen fibers of the Primary CO Membrane were irregularly distributed, with a certain space support. The surface of the collagen membrane exposed RGD by heated treatment appears tabular and smooth, while the surface of the NMBG coated Membrane exhibits an irregular coral branch-like or strip-like distribution.

Figure 2B presents the element content table of the collagen film before and after decoration. The mass percentage of the Si element increased from 8.38% to 19.91%, indicating successful attachment of NMBG to the collagen membrane. **Figure 2C** displays the fluorescence image of the content of inorganic elements such as C, N, O, Cl, P, Ca, and Si contained in BM, with the merged image of each element (**Figure 2C**).

RGD could form a bioactive interface.³¹ This not only allowed for the combination of composite biomolecules on the material to promote tissue regeneration but also provided a favorable microenvironment for wound healing. The research of Wang et al proved that multilayer material formed by NMBG exhibits biocompatibility and the ability to induce cell adhesion and migration, ensuring the delivery of nutrients and the discharge of waste during tissue regeneration.³² NMBG was applied in the compounding of organic materials to enhance their properties.^{33,34} Studies have once shown that NMBG scaffolds can support cell adhesion, proliferation, and differentiation in vitro. When in contact with body fluids in vivo, NMBG slowly released internally loaded drugs, further enhancing its biological activity.³⁵ However, most studies explored the usage of the NMBG scaffold for bone regeneration rather than its application in soft tissue healing.³⁶

In vivo Experiments Measured the Biological Effects

To further investigate the impact of BM on soft tissue wound healing, a full-thickness skin resection was made on the back of SD rats, with CO or BM applied. Images of the skin wound (**Figure 3A**) were taken on the 3rd, 7th, and 14th day after treatment with negative control (NC), CO, and BM. No signs of inflammation were observed on the wound surface. New skin growth started from the edges towards the center of the wound, resulting in a continuous reduction in the wound area. Notably, the BM group exhibited the most significant wound healing effect during the 14-day period. Particularly, by the 7th day, the wound closure rate in the BM group reached approximately 65.2%, which was

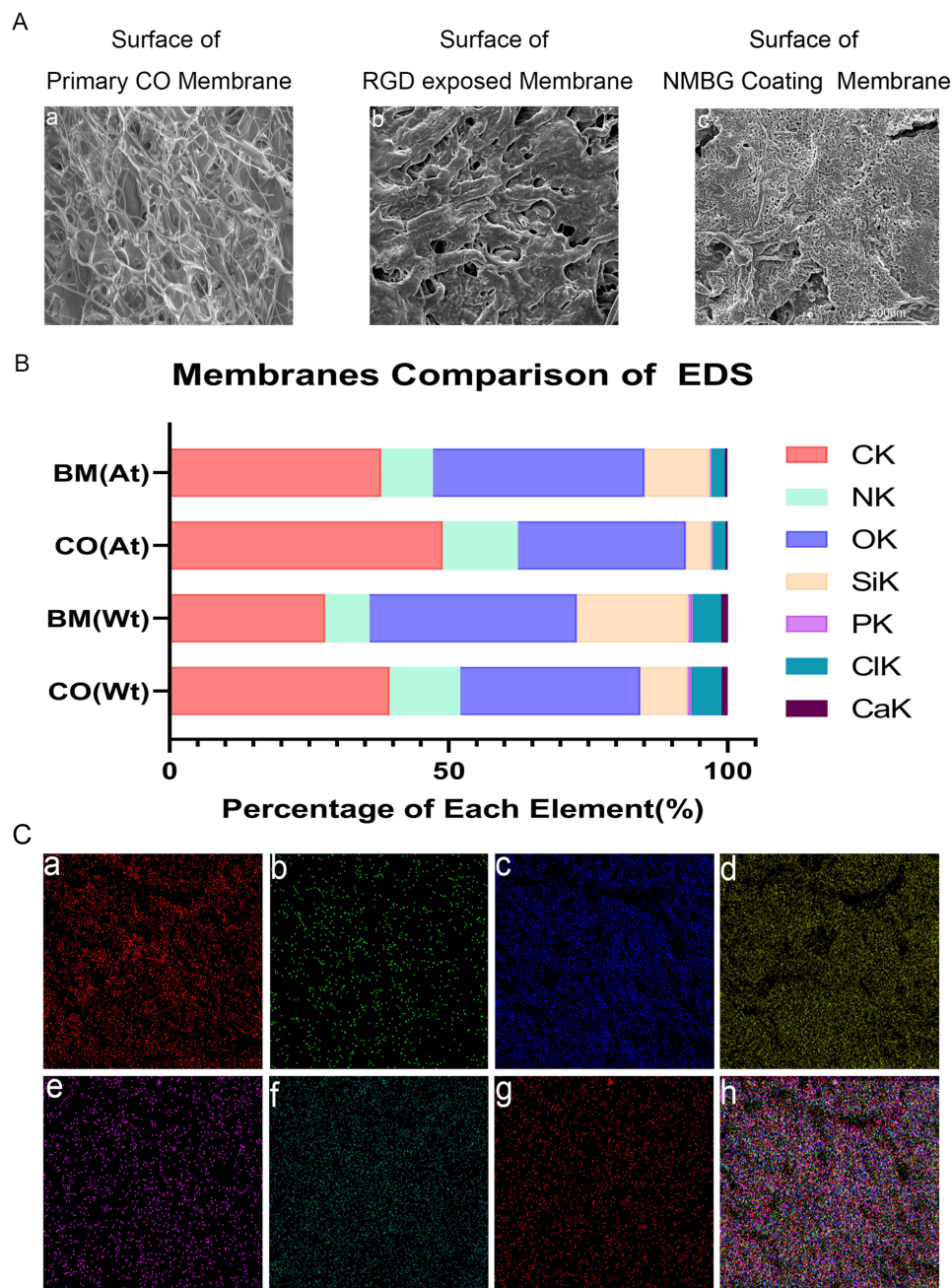


Figure 2 Morphological characterization comparison. (A) SEM scanning image of different status membranes, bar=200µm; (B) EDS: percentage of each element in membranes, before and after final modification; (C) Element content graph of BM.

significantly higher than the closure rates of 42.2% and 45.5% in the NC and CO groups, respectively ($p < 0.0001$ and $p < 0.001$). It means BM accelerated the early stage of wound healing. Furthermore, on the 14th day, **Figure 3B** demonstrates that the wound closure in the CO group was superior to that in the NC group, with statistical significance, $p < 0.0001$.

Figure 3C presents the histopathological examination of wound healing covered with different materials. H&E staining on the 14th day revealed that the wound covered with BM showed a complete formation of new epithelium, with a thicker epithelial layer compared to the BM group and CO group. The Masson staining results showed that the density of collagen fibers is highest in the BM group. These fibers were deeply stained with a regular shape, which promoted the accelerated formation of granulation tissue.

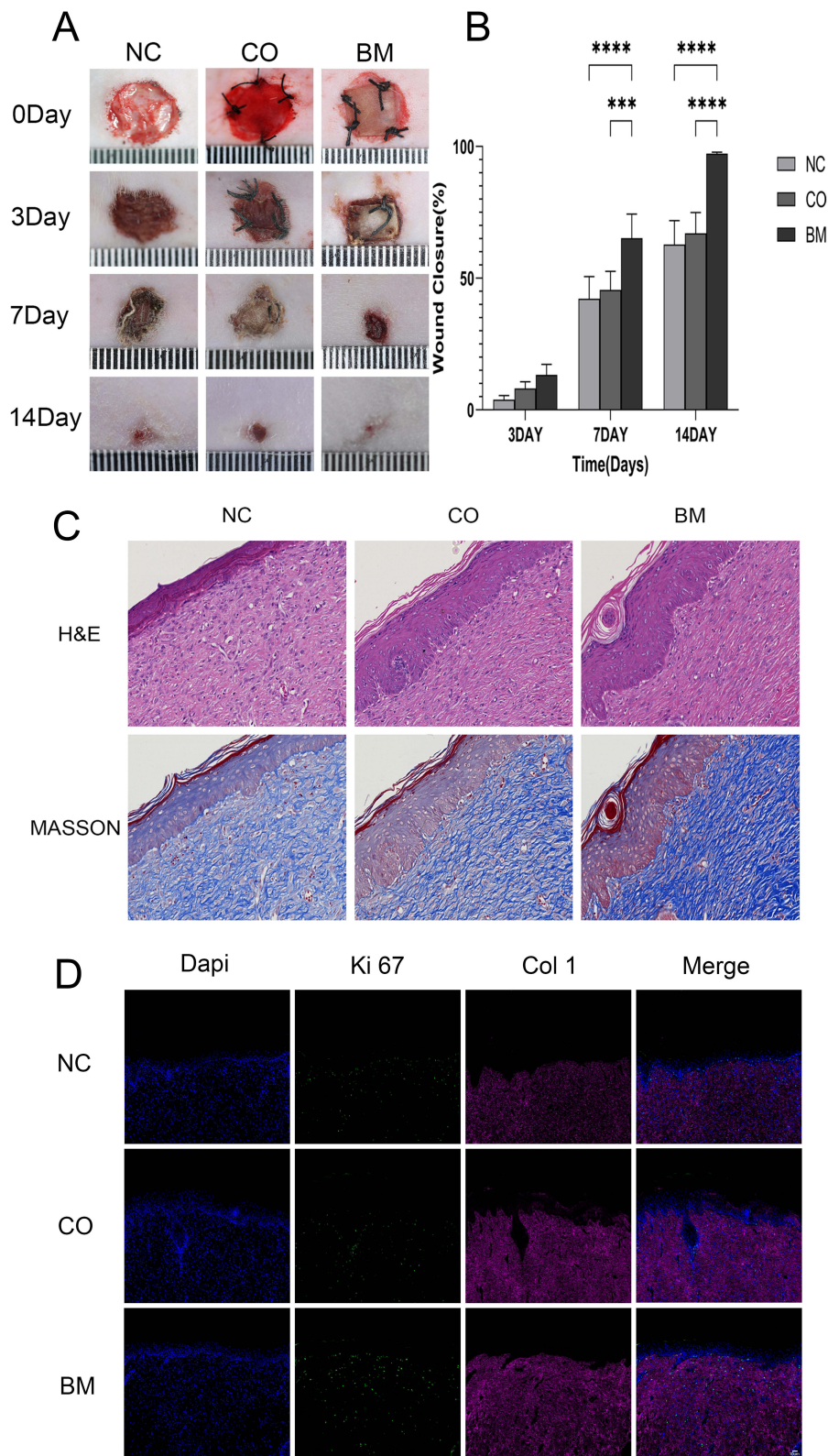


Figure 3 In vivo experiments of BM. **(A)** Wound healing among NC, CO, and BM groups on the 3rd, 7th, and 14th day; **(B)** Analyze of wound closure among NC, CO, and BM groups on the 3rd, 7th, and 14th day; **(C)** H&E and Masson staining of NC, CO and BM groups at the 14th day; **(D)** Immunofluorescence assay of Ki 67 and Col 1 among NC, CO and BM groups at the 14th day. ($P < 0.05$ was considered as statistically significant, and $*p < 0.05$, $**p < 0.01$, $***p < 0.001$, $****p < 0.0001$ in the histogram indicated that there was no statistical difference with ns or without *).

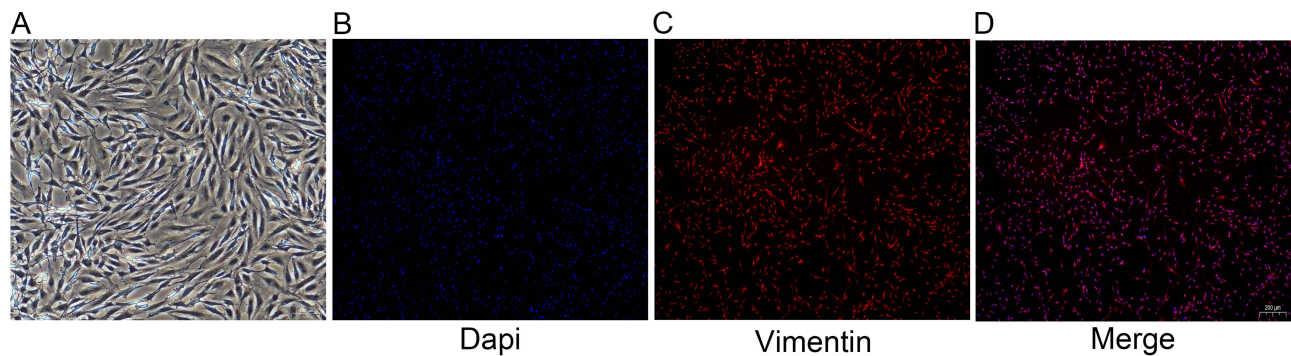


Figure 4 Skin fibroblast morphological identification. (A) SD rat primary skin fibroblasts under bright field of, bar=100um; (B–D) Immunofluorescence verification of SD rat primary skin fibroblasts, bar=200um.

The tissue immunofluorescence results (Figure 3D) of Ki 67 and Col 1 complemented the findings from the Masson staining (Figure 3C). The fluorescence intensity of Ki 67 was lower in the NC group and CO group compared to the BM group, indicating that BM was the most effective in promoting soft tissue healing among the three groups. Additionally, the fluorescence intensity of Col 1 in the BM group and CO group was relatively close and stronger than that in the NC group. This provided further evidence of the supplementary effect of the collagen component in the membrane on the extracellular matrix in connective tissue.

In vivo, studies have demonstrated that collagen promoted the migration of fibroblasts by providing a collagen supporting framework in different stages of cutaneous wound healing.³⁷ In addition, the physical sealing properties of the collagen membrane maintained a healthy physiological barrier microenvironment at the wound site, enhancing the contraction and closure of the wound during the initial stages of the wound healing process. Both CO and BM contributed to accelerating soft tissue wound healing. Furthermore, RGD has been reported to promote the adhesion and proliferation of fibroblasts, which helped create contractile forces in the wound area, primarily during the initial stages of the wound healing process.³⁸ The BM group demonstrated a strong ability to stimulate fibroblast migration and proliferation, thus promoting the healing process.

Collagen, the most crucial structural protein in the skin and a vital component of the ECM, plays an indispensable role in supporting the skeleton and facilitating the effective reconstruction of connective tissue in wounds. In Figure 3C, the MASSON staining revealed a higher accumulation of well-organized collagen fibers in the wound tissue covered with BM compared to the NC and CO groups. This suggested that the BM group had a greater deposition of collagen in ECM. Moreover, the BM group exhibited higher ECM content and parallel arrangement of collagen fibers, while the other two groups displayed loose collagen fibers with irregular arrangement. These findings, along with the data presented in Figure 3D, further confirm that the collagen component in the collagen membrane had a supplementary effect on the ECM in connective tissue.

Skin Fibroblasts' Morphological Identification

Verification of SD rat primary skin fibroblasts was conducted by assessing their morphology and immunofluorescence for Vimentin (Figure 4A–D). The purified fibroblasts were used in the cytology experiments of this study.

In vitro Experiments Measured the Biological Effects

To investigate the effect of BM on the migration of skin fibroblasts at a cellular level, migration experiments were performed via Transwell. Skin fibroblasts were observed to migrate spontaneously to the other side of the Transwell membrane. The number and fold of migrating cells in the BM group were significantly higher compared to the control group and CO group (Figure 5A–C). Cell migration is a crucial aspect of the wound healing process. The scratch experiment also (Figure 5D) demonstrated the promoting effect of BM on wound closure in vitro. At the 12th hour, indicating the initial stage of fibroblast migration, there was no significant change in the scratch curve. However, at the

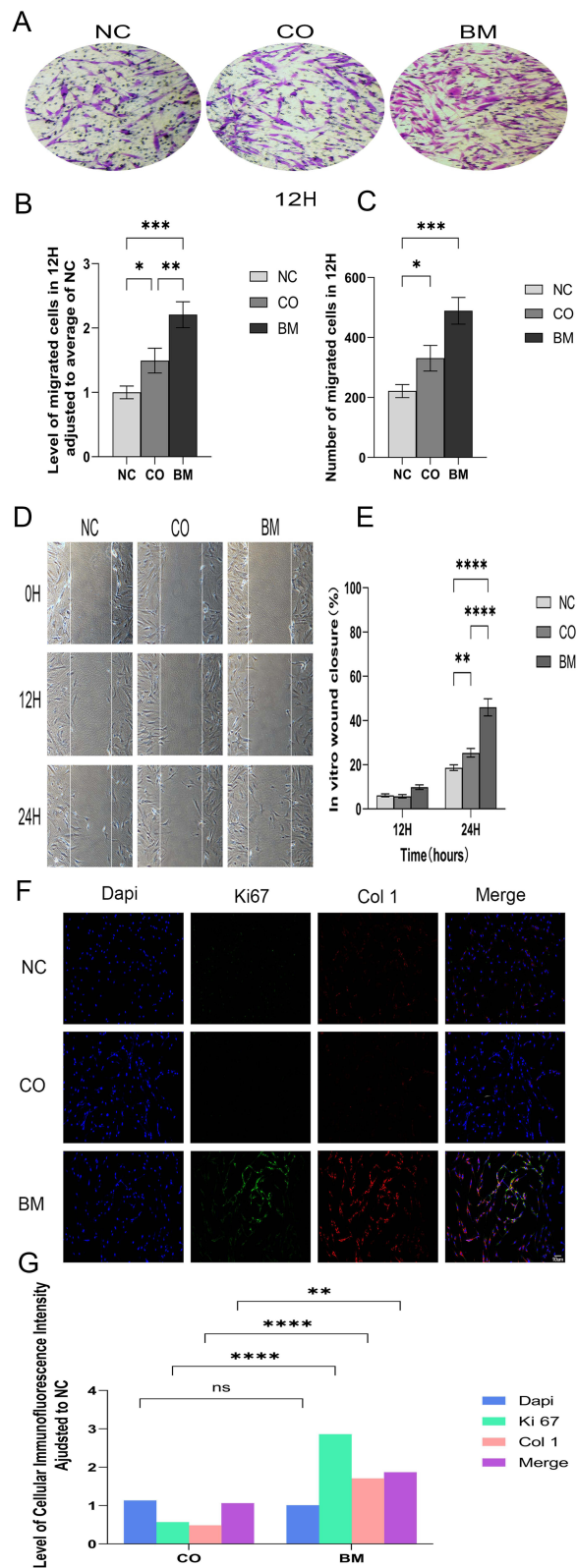


Figure 5 In vitro experiment of BM. **(A)** Skin fibroblast Transwell in NC, CO, and BM; **(B)** Analyze of skin fibroblast proliferation level in NC, CO, and BM; **(C)** Analyze of skin fibroblast proliferation number in NC, CO, and BM; **(D)** Bright field of NC, CO and BM groups at the 12th and 24th h in the Scratch; **(E)** Analyze of NC, CO, and BM groups in the Scratch; **(F)** Immunofluorescence assay of Ki 67 and Col 1 of skin fibroblast among NC, CO, and BM groups; **(G)** Analyze of NC, CO and BM groups in Immunofluorescence assay. ($P < 0.05$ was considered as statistically significant, and $*p < 0.05$, $**p < 0.01$, $***p < 0.001$, $****p < 0.0001$ in the histogram indicated that there was no statistical difference with ns or without $*$).

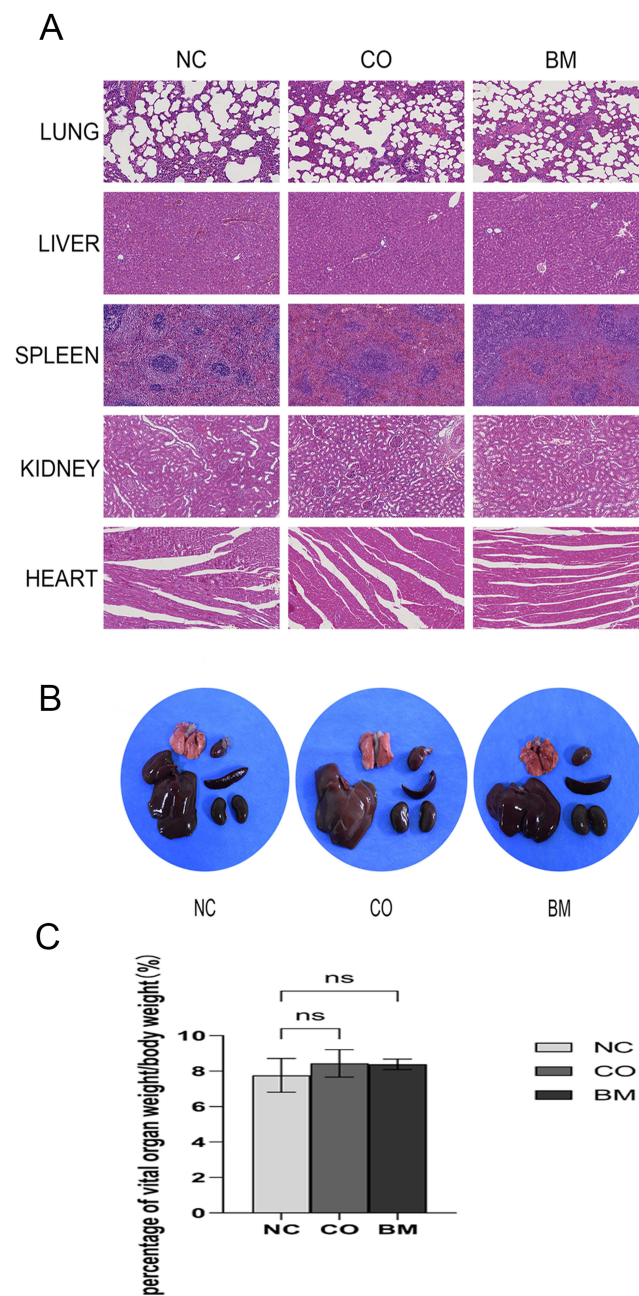


Figure 6 Detection of BM biotoxicity. **(A)** H&E staining lung, liver, spleen, kidney, and heart on the 14th day; **(B)** Color, shape, and texture presentation of vital organs on the 14th day; **(C)** Analysis of vital organs proportion compared to total weight at the 14th day. ($P < 0.05$ was considered as statistically significant, and * $p < 0.05$, ** $p < 0.01$, *** $p < 0.001$, **** $p < 0.0001$ in the histogram indicated that there was no statistical difference with ns or without *).

24th hour, the BM group exhibited the strongest migration ability among the three groups, which was statistically significant (Figure 5E). Importantly, this suggested that BM could enhance the migration capacity of fibroblast better than the CO group.

Cell immunofluorescence analysis of Ki 67 and Col 1 (Figure 5F) showed that the fluorescence intensity of Ki 67 and Col 1 was significantly lower in the NC and CO groups compared to the BM group, $p < 0.0001$ (Figure 5G). These findings meant that BM was more effective in promoting soft tissue healing compared to the other two groups.

When it turned to experiments in vitro, as depicted in Figure 5, the picture demonstrated that the BM group exhibited significantly higher cell proliferation, migration ability, secretion of main ECM components, and cell survival rate

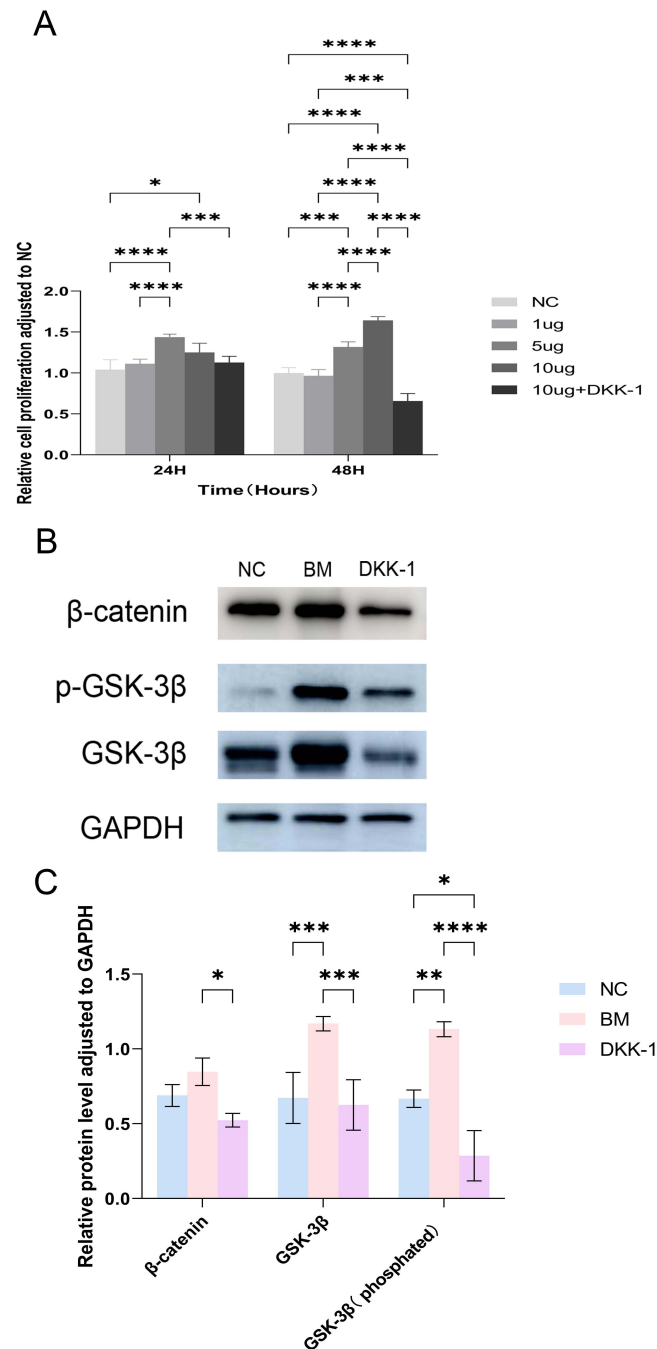


Figure 7 Activation of GSK-3β/β-catenin signaling pathway in BM. **(A)** Skin fibroblast proliferation in the NC, BM, and DKK-1 groups at the 24th and 48th h; **(B)** GSK-3β/β-catenin expression in NC, BM, and DKK-1 groups; **(C)** Analyze of β-catenin, GSK-3β, p-GSK-3β expression. ($P < 0.05$ was considered as statistically significant, and $*p < 0.05$, $**p < 0.01$, $***p < 0.001$, $****p < 0.0001$ in the histogram indicated that there was no statistical difference with ns or without *).

compared to the positive control group. A Previous study by our research group has shown that a simple collagen membrane would also enhance cell proliferation. It also indicated that the collage, along with adhesion peptides and cytokines, which provide tissue support during the healing process, can be the influential factors in the proliferation of skin fibroblasts.²⁶ These findings further supported the potential clinical applications of BM in wound healing at the cellular level.

Measurement of BM Biotoxicity

During the healing process, the local membrane could cover the wound and spread to different organs through the peripheral blood circulation system, potentially causing toxic symptoms. On the 14th day, we collected five major organs (lung, liver, spleen, kidney, and heart) from each group of experimental animals for histological evaluation using H&E staining (Figure 6A).

Analysis of the H&E stained organ sections revealed no apparent signs of toxicity in any of those tissues. When comparing the CO and BM groups with the NC group, there were no noticeable differences in the color, shape, and texture of the important organs (Figure 6B). Moreover, there was no statistically significant difference in the weight ratio of the important organs between each group on the 14th day, $p > 0.05$ (Figure 6C).

Activation of GSK-3 β / β -Catenin Signaling Axis

We investigated the effect of different concentrations of BM on cell proliferation (Figure 7A). The results demonstrated an increase in cell proliferation at the 24th h and the 48th h in the groups treated with 1, 5, and 10 μ g/mL BM. The proliferation ability of skin fibroblasts increased with the concentration of BM, with the 10 μ g/mL BM group exhibiting the highest proliferation ability. However, the addition of DKK-1 resulted in a similar cell proliferation ability to the control group (NC), but significantly lower than the group with only BM. To further investigate the inner mechanism, we conducted Western Blot experiments (Figure 7B and C) using SD rat skin cells treated with NC, BM, and DKK-1 (BM +DKK-1) groups. The results revealed that the expression of β -catenin, GSK-3 β , and p-GSK-3 β proteins was highest in the BM group, indicating that BM acted on the Wnt pathway and upregulated the expression of these proteins. Furthermore, when the Wnt pathway was blocked, even with the presence of BM, the protein contents of β -catenin, GSK-3 β , and p-GSK-3 β decreased comparing to BM group ($p < 0.05$, $p < 0.001$, and $p < 0.0001$), suggesting that RGD could activate the Wnt signaling pathway at lower concentrations, but when it came with the inhibitor of Wnt pathway, the effect of RGD reduced.

In the CCK-8 experiment (Figure 7A), DKK-1 was used as a common inhibitor of the Wnt signaling pathway. Activation of the Wnt signaling pathway inhibited the activity of GSK-3 β compounds, resulting in the accumulation of β -catenin. Then, β -catenin entered the cell nucleus and combined with the transcription factor TCF/LEF to activate the expression of target genes in proliferating cells such as Ki 67.³⁹

Previous studies have demonstrated that low concentrations of RGD could activate the Wnt signaling pathway and promote cell migration.⁴⁰ It was important to note that, under normal circumstances, activation of the Wnt pathway leads to a decrease in GSK-3 β protein expression and an increase in the expression levels of β -catenin and p-GSK-3 β proteins.⁴¹ However, since GSK-3 β was a hub gene of other signaling pathways such as PI3K/Akt, NOTCH, and so on,^{42,43} there would be some crosstalk between these pathways, resulting in similar trends in the expression levels of GSK-3 β as β -catenin and p-GSK-3 β .⁴⁴⁻⁴⁶ This suggested that when the Wnt signaling pathway was unobstructed, BM could activate Wnt to promote wound healing. Conversely, when Wnt was blocked, the potential role of BM in proliferation was significantly reduced.

Conclusion

We proposed a novel ECM-like membrane using NMBG and collagen-derived peptides, enhancing its biomaterial bioactivity. The mesoporous nanomaterials used in this study demonstrated excellent drug loading and sustained release properties due to their unique structure.⁴⁷ This approach combined surface functionalization technology and growth factor-free therapy to enhance the bioactivity of biomaterials, though researchers usually treated wound healing with growth factor, for example, Wu et al manufactured the supramolecular hydrogel microspheres of platelet-derived growth factor mimetic peptide to promote the recovery from Spinal Cord Injury.⁴⁸ The effectiveness of this method was confirmed through SEM and EDS analysis. In our research, the collagen scaffolds coated with the peptide-based and nano-mesoporous bioactive glass were found to promote the proliferation and migration of skin fibroblasts and the healing of soft tissue wounds by activating the GSK-3 β / β -catenin signaling axis. The BM facilitated fibroblasts' migration, proliferation, collagen regeneration, and the expression of Ki 67 and Col 1. The improved membrane developed in this study could be customized to accommodate different drugs, offering versatility for various clinical usage. Overall, this research presented a practical and effective bionic scaffold that held potential for clinical applications in the future.

Abbreviations

C, Carbon; N, Nitrogen; Ca, Calcium; CL, Chlorine; Si, Silicon; O, Oxygen; P, Phosphorus; HCL, Hydrochloric Acid; NMBG, Nano-mesoporous Bioactive glass; ECM, Extracellular Matrix; RGD, Arg-Gly-Asp Adhesive Peptide; FBS, Fetal Bovine Serum; BM, Bio-glass and Bio-adhesive Peptide Multiple-dressed Membrane; CO, Commercial Bio-Membrane Group (ZH-BIO Heal-all membrane); SEM, Scanning Electron Microscope; DKK-1, Dickkopf-related Protein 1; Col 3D Scaffold, 3-Dimensional Scaffold of Collage; Col 1, Collagen Type I; BFGF, Basic Fibroblast Growth Factor; IHF, Immunohistofluorescence; ICF, Immunocytofluorescence; EDS, Energy Dispersive Spectrometer.

Data Sharing Statement

Any experimental data of this study can be requested from the author.

Animal Rights and Informed Consent Statement

All procedures were approved by the Experimental Animal Care and Experimentation Committee of Ningxia Medical University (IACUC-NYLAC-2022-207, Yinchuan, Ningxia, China). The study followed ARRIVE guidelines and adhered to the 4R principles.

Acknowledgment

This work was supported by the National Natural Science Foundation of China (81860203), the Natural Science Foundation of Ningxia Province(2021AAC03336), and the Natural Science Foundation of Ningxia Province (2022BEG03160).

Disclosure

Mr. Kun Cao, Ms. Zehui Wang, Mr. Di Yan, Ms. Yanwen Liu, Ms Ting Ma, and Dr Xiaojuan Sun report a patent Material Membrane of RGD + Nanoactive Glass and Its Preparation Method and Application pending to the State Intellectual Property Office. The authors confirm that there are no other known conflicts of interest associated with our publication and no significant financial supports for the study that could influence its outcome.

References

1. Wilkinson HN, Hardman MJ. Wound healing: cellular mechanisms and pathological outcomes. *Open Biol.* 2020;10(9):200223. doi:10.1098/rsob.200223
2. Martin-Rodriguez O, Gauthier T, Bonnefoy F, et al. Pro-resolving factors released by macrophages after efferocytosis promote mucosal wound healing in inflammatory bowel disease. *Front Immunol.* 2021;12:754475. doi:10.3389/fimmu.2021.754475
3. Li B, Wang JH. Fibroblasts and myofibroblasts in wound healing: force generation and measurement. *J Tissue Viability.* 2011;20(4):108–120. doi:10.1016/j.jtv.2009.11.004
4. Cialdai F, Risaliti C, Monici M. Role of fibroblasts in wound healing and tissue remodeling on Earth and in space. *Front Bioeng Biotechnol.* 2022;10:958381. doi:10.3389/fbioe.2022.958381
5. Liddane AG, McNamara CA, Campbell MC, Mercier I, Holaska JM. Defects in emerin-nucleoskeleton binding disrupt nuclear structure and promote breast cancer cell motility and metastasis. *Mol Cancer Res.* 2021;19(7):1196–1207. doi:10.1158/1541-7786.MCR-20-0413
6. Mathew-Steiner SS, Roy S, Sen CK. Collagen in Wound Healing. *Bioengineering.* 2021;8(5):63. doi:10.3390/bioengineering8050063
7. Sharma S, Rai VK, Narang RK, Markandeywar TS. Collagen-based formulations for wound healing: a literature review [published correction appears in *Life Sci.* 2022 May 15;297:120436]. *Life Sci.* 2022;290:120096. doi:10.1016/j.lfs.2021.120096
8. Mistry K, Van Der Steen B, Vanhoecke B, et al. 791 Promoting cutaneous wound healing with nutraceutical porcine type I collagen peptides. *J Invest Dermatol.* 2020;140(7):S104–S104.
9. Heras-Parets A, Ginebra MP, Manero JM, Guillem-Martí J. Guiding Fibroblast Activation Using an RGD-Mutated Heparin Binding II Fragment of Fibronectin for Gingival Titanium Integration. *Adv Healthcare Mater.* 2023;12(21):2203307. doi:10.1002/adhm.202203307
10. Koh RH, Kim J, Kim SHL, Hwang NS. RGD-incorporated biomimetic cryogels for hyaline cartilage regeneration. *Biomed Mater.* 2022;17(2):024106. doi:10.1088/1748-605X/ac51b7
11. Li J, Zhang Y, Zhou X. Enzymatically functionalized RGD-gelatin scaffolds that recruit host mesenchymal stem cells in vivo and promote bone regeneration. *J Colloid Interface Sci.* 2022;612:377–391. doi:10.1016/j.jcis.2021.12.091
12. Chen B, Wu P, Liang L. Inhibited effect of an RGD peptide hydrogel on the expression of β 1-integrin, FAK, and Akt in Tenon's capsule fibroblasts. *J Biomed Mater Res Part B.* 2021;109(11):1857–1865. doi:10.1002/jbm.b.34847
13. Yakovlev S, Mikhailenko I, Tsurupa G, Belkin AM, Medved L. Polymerisation of fibrin α C-domains promotes endothelial cell migration and proliferation. *Thromb Haemost.* 2014;112(6):1244–1251. doi:10.1160/th14-01-0079

14. Zhang M, Yao A, Ai F, et al. Cobalt-containing borate bioactive glass fibers for treatment of diabetic wound. *J Mater Sci Mater Med.* 2023;34(8):42. doi:10.1007/s10856-023-06741-3
15. Kronick P, Maleeff B, Carroll R. The locations of collagens with different thermal stabilities in fibrils of bovine reticular dermis. *Connect Tissue Res.* 1988;18(2):123–134. doi:10.3109/03008208809008064
16. Song X, Li X, Wang F-Y, et al. Bioinspired Protein/Peptide Loaded 3D Printed PLGA Scaffold Promotes Bone Regeneration. *Front Bioeng Biotechnol.* 2022;10. doi:10.3389/fbioe.2022.832727
17. Yamada Y, Onda T, Hagiuda A, et al. RGD \times 1 X 2 motif regulates integrin α v β 5 binding for pluripotent stem cell adhesion. *FASEB J.* 2022;36(7). doi:10.1096/fj.202200317R
18. Hiratsuka T, Ogura I, Okamura A, et al. Bioresorbable bone graft composed of an RGD-enriched recombinant human collagen polypeptide induced neovascularization and regeneration of mature bone tissue. *ACS Appl Bio Mater.* 2020;3(12):8592–8602. doi:10.1021/acsabm.0c00986
19. Yang L, Yaseen M, Zhao X, et al. Gelatin modified ultrathin silk fibroin films for enhanced proliferation of cells. *Biomed Mater.* 2015;10(2):025003. doi:10.1088/1748-6041/10/2/025003
20. Huang CC, Yu M, Li H, et al. Research progress of bioactive glass and its application in orthopedics. *Adv Mater Interfaces.* 2021;8(22):2100606. doi:10.1002/admi.202100606
21. Azad Alam M, Hamed Asoushe M, Pourhakkak P, Gritsch L, Alipour A, Mohammadi S. Preparation of bioactive polymer-based composite by different techniques and application in tissue engineering: a review. *J Compos Comp.* 2021;3(3):194–205. doi:10.52547/jcc.3.3.7
22. Xiao J, Wei Q, Xue J, et al. Mesoporous bioactive glass/bacterial cellulose composite scaffolds for bone support materials. *Colloids Surf A.* 2022;642:128693. doi:10.1016/j.colsurfa.2022.128693
23. Maureira M, Cuadra F, Cádiz M, et al. Preparation and osteogenic properties of nanocomposite hydrogel beads loaded with nanometric bioactive glass particles. *Biomed Mater.* 2021;16(4):045043. doi:10.1088/1748-605X/ac0764
24. Huang S-M, Cheng Chen W, Chengchen W, et al. Synergistic effect of drug/antibiotic-impregnated micro/nanohybrid mesoporous bioactive glass/calcium phosphate composite bone cement on antibacterial and osteoconductive activities. *Biomater Adv.* 2023;152:213524. doi:10.1016/j.bioadv.2023.213524
25. Shan Z, Xie L, Liu H, et al. “Gingival Soft Tissue Integrative” lithium disilicate glass-ceramics with high mechanical properties and sustained-release lithium ions. *ACS Appl Mater Interfaces.* 2022;14(49):54572–54586. doi:10.1021/acsami.2c17033
26. Wang Z, Cao K, Yan D, et al. A study of the role of multiple layer-by-layer assembled bionic extracellular matrix in promoting wound healing via activation of the Wnt signaling pathway. *J Biomed Mater Res B Appl Biomater.* 2023;111(6):1159–1170. doi:10.1002/jbm.b.35222
27. Zhou N, Xiaoe M, Wusheng H, et al. Effect of RGD content in poly(ethylene glycol)-crosslinked poly(methyl vinyl ether-alt-maleic acid) hydrogels on the expansion of ovarian cancer stem-like cells. *Mater Sci Eng C.* 2021;118:111477. doi:10.1016/j.msec.2020.111477
28. Pond KW, Doubrovinski K, Thorne CA. Wnt/ β -catenin signaling in tissue self-organization. *Genes.* 2020;11(8):939. doi:10.3390/genes11080939
29. Davis GE. Affinity of integrins for damaged extracellular matrix: alpha v beta 3 binds to denatured collagen type I through RGD sites. *Biochem Biophys Res Commun.* 1992;182(3):1025–1031. doi:10.1016/0006-291X(92)91834-D
30. Taubenberger AV, Woodruff MA, Bai H, Muller DJ, Huttmacher DW. The effect of unlocking RGD-motifs in collagen I on pre-osteoblast adhesion and differentiation. *Biomaterials.* 2010;31(10):2827–2835. doi:10.1016/j.biomaterials.2009.12.051
31. Pan G, Shinde S, Yeung SY, et al. An epitope-imprinted biointerface with dynamic bioactivity for modulating cell-biomaterial interactions. *Angew Chem Int Ed Engl.* 2017;56(50):15959–15963. doi:10.1002/anie.201708635
32. Wang S, Huang G, Dong Y. Directional migration and odontogenic differentiation of bone marrow stem cells induced by dentin coated with nanobioactive glass. *J Endod.* 2020;46(2):216–223. doi:10.1016/j.joen.2019.11.004
33. Kumari S. Multifunctional organic and inorganic hybrid bionanocomposite of chitosan/poly(vinyl alcohol)/nanobioactive glass/nanocellulose for bone tissue engineering. *J Mech Behav Biomed Mater.* 2022;135:105427. doi:10.1016/j.jmbm.2022.105427
34. Lee MJ, Kim MJ, Mangal U, Seo JY, Kwon JS, Choi SH. Zinc-modified phosphate-based glass micro-filler improves Candida albicans resistance of auto-polymerized acrylic resin without altering mechanical performance. *Sci Rep.* 2022;12(1):19456. doi:10.1038/s41598-022-24172-y
35. El-Okaily MS, El-Rafei AM, Basha M, et al. Efficient drug delivery vehicles of environmentally benign nano-fibers comprising bioactive glass/chitosan/polyvinyl alcohol composites. *Int J Biol Macromol.* 2021;182:1582–1589. doi:10.1016/j.ijbiomac.2021.05.079
36. Cheng Y, Li Y, Huang S, et al. Hybrid freeze-dried dressings composed of epidermal growth factor and recombinant human-like collagen enhance cutaneous wound healing in rats. *Front Bioeng Biotechnol.* 2020;8:742. doi:10.3389/fbioe.2020.00742
37. Pajic-Lijakovic I, Milivojevic M, Clark AG. Collective cell migration on collagen-I networks: the impact of matrix viscoelasticity. *Front Cell Dev Biol.* 2022;10:901026. doi:10.3389/fcell.2022.901026
38. Yamada Y, Onda T, Wada Y, Hamada K, Kikkawa Y, Nomizu M. Structure-activity relationships of RGD-containing peptides in integrin α v β 5-mediated cell adhesion. *ACS Omega.* 2023;8(5):4687–4693. doi:10.1021/acsomega.2c06540
39. Andrés-Sánchez N, Fisher D, Krasinska L. Physiological functions and roles in cancer of the proliferation marker Ki-67. *J Cell Sci.* 2022;135(11):jcs258932. doi:10.1242/jcs.258932
40. Wang Y, He J, Zhang J, Zhang N, Zhou Y, Wu F. Cell migration induces apoptosis in osteosarcoma cell via inhibition of Wnt- β -catenin signaling pathway. *Colloids Surf B Biointerfaces.* 2023;223:113142. doi:10.1016/j.colsurfb.2023.113142
41. Gao S, Wang S, Zhao Z, et al. TUBB4A interacts with MYH9 to protect the nucleus during cell migration and promotes prostate cancer via GSK3 β / β -catenin signalling. *Nat Commun.* 2022;13(1):2792. doi:10.1038/s41467-022-30409-1
42. Liu M, Huang X, Tian Y, et al. Phosphorylated GSK-3 β protects stress-induced apoptosis of myoblasts via the PI3K/Akt signaling pathway. *Mol Med Rep.* 2020;22(1):317–327. doi:10.3892/mmr.2020.11105
43. Wei D, Zhu X, Li S, et al. Tideglusib suppresses stem-cell-like features and progression of osteosarcoma by inhibiting GSK-3 β /NOTCH1 signaling. *Biochem Biophys Res Commun.* 2021;554:206–213. doi:10.1016/j.bbrc.2020.12.055
44. Ren C, Chen X, Du N, et al. Low-intensity pulsed ultrasound promotes Schwann cell viability and proliferation via the GSK-3 β / β -catenin signaling pathway. *Int J Biol Sci.* 2018;14(5):497–507. doi:10.7150/ijbs.22409
45. Chen B, Li X, Wu L, et al. Quercetin suppresses human glioblastoma migration and invasion via GSK3 β / β -catenin/ZEB1 signaling pathway. *Front Pharmacol.* 2022;13:963614. doi:10.3389/fphar.2022.963614

46. He J, Wang M, Yang L, et al. Astragaloside IV alleviates intestinal barrier dysfunction via the AKT-GSK3 β -catenin pathway in peritoneal dialysis. *Front Pharmacol.* 2022;13:873150. doi:10.3389/fphar.2022.873150
47. Ma R, Su Y, Cao R, Wang K, Yang P. Enhanced osteogenic activity and bone repair ability of PLGA/MBG scaffolds doped with ZIF-8 nanoparticles loaded with BMP-2. *Int J Nanomed.* 2023;18:5055–5072. doi:10.2147/IJN.S423985
48. Wu W, Jia S, Xu H, et al. Supramolecular hydrogel microspheres of platelet-derived growth factor mimetic peptide promote recovery from spinal cord injury. *ACS Nano.* 2023;17(4):3818–3837. doi:10.1021/acsnano.2c12017

International Journal of Nanomedicine

Dovepress

Publish your work in this journal

The International Journal of Nanomedicine is an international, peer-reviewed journal focusing on the application of nanotechnology in diagnostics, therapeutics, and drug delivery systems throughout the biomedical field. This journal is indexed on PubMed Central, MedLine, CAS, SciSearch[®], Current Contents[®]/Clinical Medicine, Journal Citation Reports/Science Edition, EMBase, Scopus and the Elsevier Bibliographic databases. The manuscript management system is completely online and includes a very quick and fair peer-review system, which is all easy to use. Visit <http://www.dovepress.com/testimonials.php> to read real quotes from published authors.

Submit your manuscript here: <https://www.dovepress.com/international-journal-of-nanomedicine-journal>